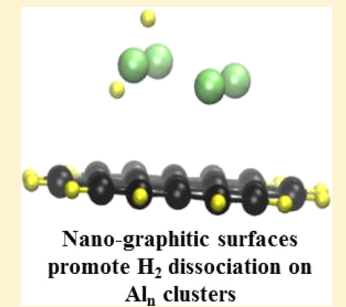
pubs.acs.org/JPCC

Promoting Effect of Carbon Surfaces on H₂ Dissociation on Al_n **Clusters by First Principles Calculations**

Francesca Costanzo,* Marc C. van Hemert, and Geert-Jan Kroes

Gorlaeus Laboratories, Leiden Institute of Chemistry, P.O. Box 9502, 2300 RA Leiden, The Netherlands

ABSTRACT: Recent experiments show that carbon nanomaterials, such as carbon nanofibers, may be used to catalyze the dehydrogenation and rehydrogenation of hydrogen storage materials, such as the benchmark complex metal hydride NaAlH₄. However it is not clear how the carbon material can accomplish the dissociation (or recombination) of H_2 . In this work we investigate the dissociation of H_2 on Al_n (n = 2, 4, and 6) clusters supported by coronene and graphene substrates using density functional theory (DFT), where coronene and graphene are taken as models for nanographitic surfaces. In our calculations, we account for van der Waals interactions by adapting the correlation part of the PBE exchange-correlation functional with the Grimme and Langreth corrections, and we use NEB to calculate the minimum energy reaction path for the dissociation of H₂. Analysis of the minimum barrier reaction paths and the associated dissociation barriers of H₂ on Al_n clusters interacting with the modeled carbon



surfaces shows that the investigated carbon materials have a promoting effect on the dissociation of H₂ on the Al_n clusters, resulting in barrierless dissociation of H₂ on Al₄ and Al₆ supported on coronene. The calculations on coronene suggest that the promoting effect comes from a stabilization of the singlet states of Al_n.

I. INTRODUCTION

Efficient hydrogen storage is an essential prerequisite for the use of hydrogen as an automobile fuel. 1,2 Physical storage of hydrogen as highly pressurized gas or in the liquid phase at low temperature is associated with high volume,³ energy losses,^{2,3} and significant safety risks.⁴ Physical adsorption of hydrogen onto lightweight materials, such as clathrate hydrates,⁵ metal organic frameworks,⁶ and carbon nanotubes,⁷ may only results in high storage densities at cryogenic temperatures. The alternative is chemical storage: the preferably reversible absorption of hydrogen into another material.

Alanates of light alkali metals⁸⁻¹⁰ like sodium alanate (NaAlH₄), with its fairly low H₂ desorption temperature, form a promising class of systems for reversible hydrogen storage in vehicle and portable applications. 11-13 During the past few years intensive research on alkali-metal aluminum hydrates has been carried out, but the thermodynamic properties and unfavorable kinetics still remain a problem.

Important early progress was made by Bogdanović et al., 14,15 who showed that reversible hydrogenation cycling is feasible in sodium alanate by adding titanium based catalysts. 16 This result was followed by further progress in synthetic methodology and characterization of sodium alanate doped with Ti. 17,18 Ti additives improve the kinetics of hydrogen absorption and desorption, but high pressure (P > 100 bar) and long times are still needed to reload depleted doped sodium alanate. The quest to establish the mechanism by which Ti and other transition metals promote reversible hydrogen uptake and release from NaAlH₄ remains an area of active research. 16,19-22 In these experiments, the presence of NaCl and traces of Ti/Al alloys have been detected, implying that a zero valent Ti precursor has taken part in the chemical reaction.

A different strategy to improve the kinetics and thermodynamics for hydrogenation/dehydrogenation of NaAlH4 is to use nanosized NaAlH₄ particles supported on carbon nanostructures. 23,24 Berseth et al. used a solvent preparation technique to intimately mix the NaAlH4 and carbon materials without introducing metal contaminants. By experiments and first principles calculations, they showed that the energies to remove a hydrogen atom from NaAlH₄ supported on C₆₀ fullerene, carbon nanotubes, and graphene are smaller than those in the pure alanate, and are close to the energies calculated for alanates doped with Ti. Moreover, no structural changes of the carbon nanostructures take place, so that the carbon materials behave as true catalysts. The weakening of the metal-hydrogen (Al-H) bond leads to lowering of the hydrogen desorption energy and hence to improved kinetics.

In other experiments, 25,24 nanosized NaAlH₄ particles supported on a carbon nanofiber displayed improved hydrogen absorption and desorption characteristics compared to bulk alanates. The hydrogen desorption temperature decreased considerably and significant amounts of hydrogen could be desorbed at T < 160 °C. An enhancement was also observed in the reloading of materials, and hydrogen storage became partially reversible. Moreover, it was shown²⁶ how the adsorption behavior of NaH and NaAlH4 is influenced by intimate contact with nanoporous carbon. It was found that not only faster kinetics are observed but also a shift in the equilibrium conditions, which is at least partly due to reversible interaction between Na and the carbon matrix.

Received: October 23, 2013 Revised: December 10, 2013 Published: December 11, 2013 Recently Gao et al.²⁷ studied the reversibility of hydrogen adsorption in NaAlH₄ carbon composites and the factor which limits the reversibility. They found that reversibility can be achieved by adding extra Na, avoiding the formation of NaH and lowering the dehydrogenation temperature.

Several attempts have been made to understand the role played by aluminum in the overall process. For example, Moc²⁸ showed that the hydrogenation reaction on singlet Al₆ is described by a lack of activation barrier for H₂ cleavage (at 0 K), consistent with gas phase experiments. Moc²⁹ studied also the reaction paths of Al₂ with H₂ using B3LYP DFT, high level single-reference and CASSCF based ab initio methods, verifying that B3LYP accounts properly for dynamic correlation. In addition, a recent theoretical work³⁰ showed how the shape, the number of atoms, and the electronic spin state of small aluminum clusters can drastically change the ability to dissociate and bind hydrogen molecules.

Starting from these interesting results, our goal is to study, by density functional theory (DFT) calculations, the combined effect that Al_n clusters (n=2,4, and 6) and carbon surfaces have on the dissociation of the hydrogen molecule, using coronene and graphene as model systems for nanographitic materials (alternatively, coronene may be viewed as a model system for graphene). We demonstrate the promoting effect that carbon surfaces have on H_2 dissociation on Al_n clusters, with even zero activation energy for H_2 on Al_4 and Al_6 on coronene. This result can be explained by analysis of the molecular orbitals involved, the charge transfer, and the electrostatic energy. The choice of the Al_n clusters with n even is based on Kawamura's work, n who demonstrated that n is likely to be dissociated on even atom small clusters; this also was confirmed by our earlier work on bare Al_n clusters.

Taking into account that the spin state and the cluster size of the Al_n are important to the dissociation of the H_2 molecule, ³⁰ we started our calculation with coronene, a finite molecule for which it is easy to establish the spin multiplicity. We chose the coronene molecule as a model for extended carbon surfaces such as graphene, and to mimic the edge (defect) of nanocarbon surfaces. This paper is organized as follows: in section II the description of the applied methods is given. In section III results and discussion are reported beginning with those for the bare aluminum clusters (section A), followed by for aluminum clusters supported by coronene and graphene surfaces (section B). Section C contains results on chemisorbed states of H₂ on Al_n supported by coronene and graphene surfaces. Section D concludes the results section with a presentation of the dissociation of H₂ on Al_n supported by carbon materials. Section IV concludes the paper.

II. METHODS

A. DFT Calculations. We performed periodic DFT calculations using the Quantum-ESPRESSO package.³² Ultrasoft pseudopotentials were adopted and the Kohn–Sham wave functions were expanded in a plane-wave basis set with an energy cutoff of 462.59 eV, while a cutoff of 2775.56 eV was applied to the charge density. Periodic boundary conditions were used with 2 k points along each of the x and y directions for the Brillouin zone integration. The generalized gradient approximation (GGA) was used for the exchange-correlation energy, using the PBE functional.³³ To model the graphene (G) surface, a periodically repeated slab with a single layer of 32 C atoms was chosen. The symmetry of the cell was hexagonal, with parameters a = b = 9.88 Å and c = 24.61 Å. For the

electronic part, we used "smearing" occupation with a Fermi-Dirac function. 34

To model the coronene molecule (C) we used a cubic cell, accounting for the symmetry of the system, with a = b = c =21.17 Å, and α , β , $\gamma \approx 90^{\circ}$. For the C molecule additional calculations were performed with the CP2K program³⁵ with GTH pseudopotentials,³⁶ hybrid plane wave/Gaussian type orbital (PW/GTO) basis functions, and the PBE functional; and with the G03 program³⁷ using the 6-31-G(d,p) (GTO) basis sets and B3LYP hybrid density functional. 38,39 Notice that, since the potential energy surface is quite flat for the Al_n-C systems, different local minima can be obtained depending on the functional used. The spin unrestricted Kohn-Sham formalism was used for calculations on triplet states. We use two different methodological approaches, which use plane waves (Quantum-ESPRESSO) and localized wave functions (CP2K), in accordance with the different nature of the two systems: periodic (graphene) and finite (coronene). To characterize the reaction pathway going from physisorption to chemisorption of H₂ on aluminum clusters interacting with a C or G surface, we computed minimum energy pathways and activation barriers using the nudge elastic band (NEB) method.⁴⁰ The NEB program is implemented in Quantum-ESPRESSO, so all calculations were perfomed with the same features used in the geometry optimizations. During the NEB simulations, we used the quasi-Newton optimization scheme from Broyden.41 We chose seven images to describe our reaction path profile and auto climbing images to describe the transition state. The elastic constants related to the springs used to mimic the elastic band were 29.15 and 19.44 eV/Å² for k_{max} and k_{\min} , respectively. The threshold value of the norm of the force orthogonal to the path, chosen to reach the convergence in the simulation, was 0.1 eV/Å.

A known drawback of standard DFT methods is their failure to describe van der Waals (vdW) interactions, in particular the leading term $-C_6/R^6$, which results from dipole-dipole electron correlation effects. Here we applied vdW corrections with the so-called "seamless" vdW-DF method, 42 based on nonlocal dispersion energy functionals and with the semiempirical PBE-D2 method.⁴³ The PBE approach corrected by including vdW-DF has been recently applied to describe the binding/diffusion of hydrogen atom on graphene. 44,45 We choose to use PBE rather than rev-PBE since it was found in recent studies of molecules interacting with metals that the interaction potential became too repulsive when using RevPBE. 46 PBE exchange combined with the vdW-DF correlation functional has been used successfully to model adsorption of molecules to metal surfaces. 47-51 Although it is shown that screening and polarization effects are important for specific classes of systems such as interactions between nanoparticles⁵² and between molecules and metal surfaces, ^{53,54} we did not consider the use of a method incorporating these effects⁵³ because it is at present unclear whether this would lead to improvements for the systems we consider here.

III. RESULTS AND DISCUSSION

A. Al_n Clusters. Al_n clusters have already been extensively studied with accurate quantum chemical methods. ^{28–30,55} It is difficult to assess which computational method is most appropriate for nanoaluminum because there are only limited experimental data available for small neutral clusters (for Al₂ and Al₃). ^{56–58}

In order to choose the best method to model H_2 on Al_n clusters on a G surface, we begin by modeling Al_n clusters with n=2,4,6. We performed DFT calculations with the B3LYP and PBE functionals. The B3LYP functional has been shown to provide a very accurate description of the electronic structure and the structures of Al_n clusters. $^{28-30,55}$ We therefore use it as a reference for our calculations on Al_n clusters. vdW forces are accounted for by adapting the correlation part of the PBE XC functional using the methods of Langreth et al. 42 and Grimme. 43 We called the adapted functionals vdW-DF and PBE-D2, respectively.

Table 1. Binding Energies (eV) at the DFT Level, Calculated with Various Basis Sets and Functionals for Al_n with 2, 4, and 6 Atoms^a

system	basis	functional	$E_b(eV)$	E_{diss}
¹ Al ₂	hybrid GTO/PW	PBE-D2	-0.54	
	PW	PBE	-0.70	
	PW	vdW-DF	-0.57	
	6-31G(d,p)	B3LYP	-0.47	
$^{3}\text{Al}_{2}$	hybrid GTO/PW	PBE-D2	-0.83	-1.66
	6-31G(d,p)	B3LYP	-0.66	-1.32
	6-31+G(d)	B3LYP		-1.31
	experiment			-1.36
$^{1}\text{Al}_{4}$	hybrid GTO/PW	PBE-D2	-1.57	
	PW	PBE	-1.42	
	PW	vdW-DF	-1.16	
	6-31G(d,p)	B3LYP	-1.19	
$^{3}\text{Al}_{4}$	hybrid GTO/PW	PBE-D2	-1.64	-6.56
	6-31G(d,p)	B3LYP	-1.23	-4.92
	6-31+G(d)	B3LYP		-4.94
$^{1}\text{Al}_{6}$	hybrid GTO/PW	PBE-D2	-2.06	
	PW	PBE	-1.85	
	PW	vdW-DF	-1.49	
	6-31G(d,p)	B3LYP	-1.58	
³ Al ₆ octahedral	hybrid GTO/PW	PBE-D2	-2.07	-12.42
	6-31G(d,p)	B3LYP	-1.56	-9.36
	6-31+G(d)	B3LYP		-9.22
³ Al ₆ tent	hybrid GTO/PW	PBE-D2	-2.05	
	GTO	B3LYP	-1.58	

[&]quot;See Figure 1. The experimental values and the dissociation energies $(E_{\rm diss})$ at the B3LYP level with 6-31+G(d) basis sets are taken from ref 55.

Table 1 reports the binding energies (E_b) and the dissociation energies (E_{diss}) for the Al_n clusters, calculated by eqs 1 and 2, respectively.

$$E_{\rm b} = E_{\rm Aln}/n - E_{\rm Al} \tag{1}$$

$$E_{\rm diss} = E_{\rm b} n \tag{2}$$

The $E_{\rm b}$ accounts for the cohesive energy, that is, the stability per atom upon cluster formation. It can be determined experimentally from the enthalpy of sublimation at 0 K. SE $E_{\rm diss}$ in eq 2 is the energy needed to dissociate the cluster into atoms and is reported only for the ground states of the clusters.

In Table 1 we also make a comparison with plane wave (PW) calculations, localized functional (GTO) calculations, experimental values when available, and results of earlier calculations. ⁵⁵

As previously found from very accurate calculations (CCSD-(T) and CCI/QZ), 30,55 the triplet state is favored with respect to the singlet state for Al_2 and Al_4 , while Al_6 shows almost identical values of the energies of the lowest singlet and triplet states.

For the singlet states a good agreement is found between the $E_{\rm b}$ computed with the B3LYP and vdW-DF functionals. For Al₂ in the triplet state we found a good agreement of the $E_{\rm diss}$ from our B3LYP calculations with the values reported in ref 55. and experimental values. Our $E_{\rm diss}$ values are also in good agreement with the calculations from Pino et al.³⁰ at the DFT/B3LYP/6-311+G* level of theory. Unfortunately, a comparison of our calculated $E_{\rm diss}$ with experiment for Al clusters with n > 2 is not possible due to a lack of experimental data, but there is good agreement between our B3LYP calculations and the ones reported in the literature⁵⁵ at higher levels of theory for all the clusters studied.

In contrast, the agreement between the PBE-D2 and B3LYP functional results is quite poor, especially for the triplet state. As already experienced for similar systems, ^{59,60} the PBE-D2 corrected functional, which is based on a semiempirical approach, tends to overestimate binding energies.

The calculated geometries of the lowest singlet states of the Al_n are drawn in Figure 1. We found for Al_4 a planar structure as lowest state, while Al_6 presents a three-dimensional structure with various isoenergetic minima, in agreement with the literature. Finally the calculated Al-Al distances are reported in the last column of Table 2 and also are in good agreement with values reported in the literature.

B. Interaction of Al_n Clusters with Carbon Materials. In recent years cluster-based materials have been a subject of intensive research due to both fundamental and technological

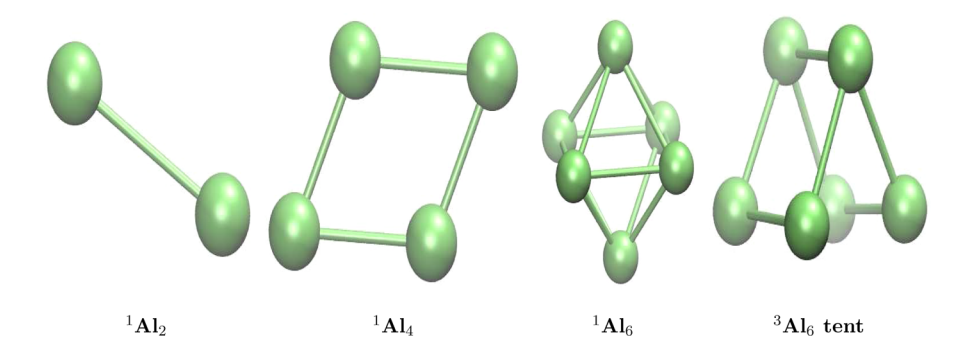


Figure 1. Al_n with n = 2, 4, and 6 atoms. For Al_6 also the tent conformation of the triplet state is drawn.

Table 2. Distances (Å) for H₂ Chemisorbed on Al_n Clusters Interacting with C and G, Drawn in Figures 5 and 6, Respectively^a

	Al-Al	Al-C	H–Al	Н-Н	Al-Al (Al _n)
¹ Al ₂ -C	2.81	2.09			3.10
$^{3}\text{Al}_{2}\text{-C}$	2.66	2.41			2.76
H_2 - Al_2 - C	2.80	2.27	1.84, 1.74	2.21	
planar dibridged ^b	2.99		1.83		3.10
$^{1}Al_{4}-C$	2.66	2.82			2.48
$^{3}Al_{4}-C$	2.60	3.69			2.56
H_2 - Al_4 - C	2.54	2.97	1.78, 1.75	2.24	2.48
planar dibridged ^b	2.76		1.98, 1.76		2.48
¹ Al ₆ -C	2.71	3.68			2.57
$^{3}Al_{6}-C$	2.71	3.65			2.55
H_2 - Al_6 - C	2.57	3.25	1.78, 1.90	2.15	2.57
dibridged ^b	2.67		1.89, 1.91		2.57
Al ₂ -G	2.92	2.38			3.10
H_2 - Al_2 - G	2.54	3.89	1.80, 1.80	2.13	3.10
planar dibridged ^b	2.99		1.83		3.10
Al ₄ –G	2.60	4.01			2.48
H_2 - Al_4 - G	2.50	3.70	1.59, 1.74	4.72	2.48
$2'$ -monobridged b	2.52		1.69, 1.92		2.48
Al ₆ –G	2.70	4.10			2.57
H_2-Al_6-G	2.62	3.90	1.90, 1.89	2.23	2.57
dibridged ^b	2.67		1.89, 1.91		2.57

^aDistances for the bare Al_n clusters are reported in the last column. ^bValues related to the Al_nH_2 configurations (without carbon support) taken from ref 30.

importance. 61,62 Here we study the interaction of the Al_n cluster with two substrates, i.e., the C molecule and the G surface, as models for nanographitic surfaces. We show that the structure and electronic properties of the aluminum clusters depend on their sizes and that the carbon support affects the energy dissociation barrier of the H_2 molecule.

C is a finite molecule and is easier to treat computationally than the G surface. As we explain later, the interaction of

coronene with Al_n clusters stabilizes the singlet state over the triplet state for any cluster size studied, so only the singlet state configurations are reported in Figure 2.

Figure 2 shows the minimum energy structures obtained by geometry optimization of Al₂-C, Al₄-C, and Al₆-C. Table 2 reports the Al-Al and the Al-C distances for all the geometries optimized using the vdW-DF functional with PW basis functions and using the PBE-D2 functional, in conjunction with hybrid PW/GTO, for the Al_n-G and Al_n-C systems, respectively. The reference Al-Al distance in the bare Al, cluster is reported in the last column. In the geometry optimized Al₂-C system, Al₂ is located toward the extremity of the C molecule. This preferred location arises from the electric field gradient created by a circle of C atoms surrounded by H atoms. The Al-Al distance decreases from 3.10 Å for the bare cluster to 2.81 Å, the coronene C-C bond distances underneath the Al₂ increase to 1.44 Å with an Al–C distance of 2.09 Å, suggesting a strong covalent bond, and the C molecule deviates 24° from planarity.

The Al_4 –C and Al_6 –C cases present different scenarios. The Al_4 cluster resides above the center of coronene after the geometry optimization, with the Al–Al distances longer (2.66 Å) than in the bare Al_n cluster (2.48 Å), and a much longer Al–C distance at 2.82 Å. For the Al_6 –C system, the conformation of the Al_6 does not change with respect to the isolated cluster, keeping the three-dimensional structure of the bare cluster but trying to match at least two Al atoms with corresponding C atoms of the coronene, with an even larger Al–C distance of 3.68 Å, and with the Al–Al distance equal to 2.71 Å.

The Al–C distances and the elongation of the C–C bond in the coronene molecule suggest for Al_4 –C and Al_6 –C a mixed physi-chemisorbed interaction. Table 3 shows the binding energies calculated for the Al_n cluster interacting with the C molecule and the G surface, respectively. Binding energies (E_b) are calculated from eq 3 using the vdW-DF functional with PW basis functions and the PBE-D2 functional with a hybrid PW/GTO basis set, for the Al_n –G and Al_n –C systems, respectively

$$E_{\rm b} = E_{\rm Aln-S} - E_{\rm Aln} - E_{\rm S} \tag{3}$$

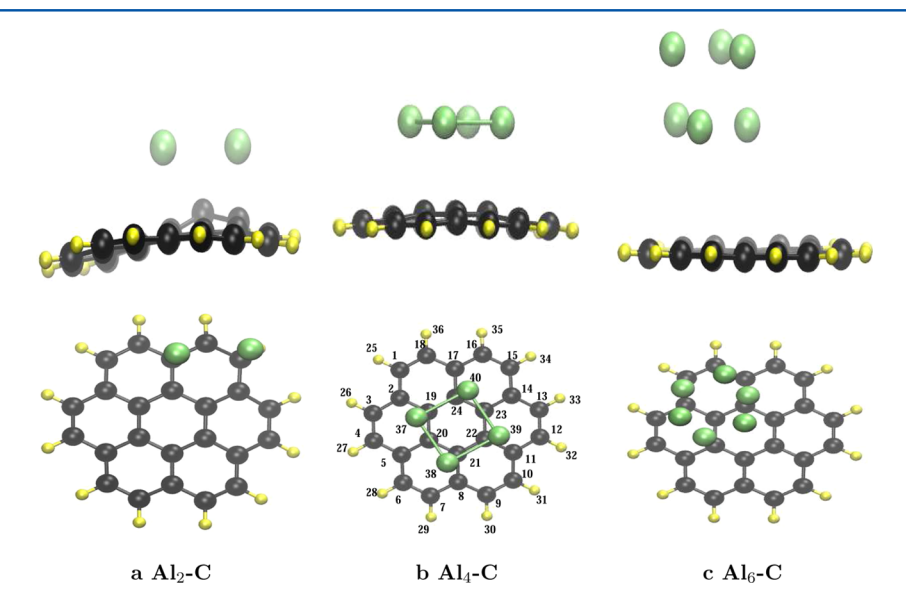


Figure 2. Al_n with n = 2, 4, and 6 atoms interacting with coronone (C). Side and top views are shown. Black, light gray (yellow), and dark gray (green) balls correspond to the C, H, and Al atoms, respectively.

Table 3. Binding Energies (eV) Calculated by eq 3 and Obtained with the PBE-D2 Functional, Using Hybrid PW/GTO and with the vdW-DF Functional, Using PW Basis Functions, for Al_n-C and Al_n-G Systems, Respectively^a

	Al_n -C	Al_n-G
$^{1}\mathrm{Al}_{2}$	-1.65	-0.41
3 Al $_{2}$	-0.81	
$^{1}Al_{4}$	-0.75	-0.66
$^{3}\text{Al}_{4}$	-0.36	
$^{1}\text{Al}_{6}$	-0.47	-0.55
$^{3}\text{Al}_{6}$	-0.19	

^aAll of the configurations are drawn in Figures 1, 2, and 4.

where S is either the C molecule or the G surface.

We now first discuss the interaction with the C molecule as a model for the interaction with the G surface. The interaction of coronene with Al_n clusters stabilizes the singlet state over the triplet state for any cluster size studied. This singlet over triplet stabilization can, at least in part, be explained by a charge transfer from the Al atoms to the carbon atoms of the coronene molecule. This is quite evident for $\mathrm{Al}_2\mathrm{-C}$ and $\mathrm{Al}_4\mathrm{-C}$. Here we discuss only the case of the $\mathrm{Al}_4\mathrm{-C}$ system. Figure 3 shows the

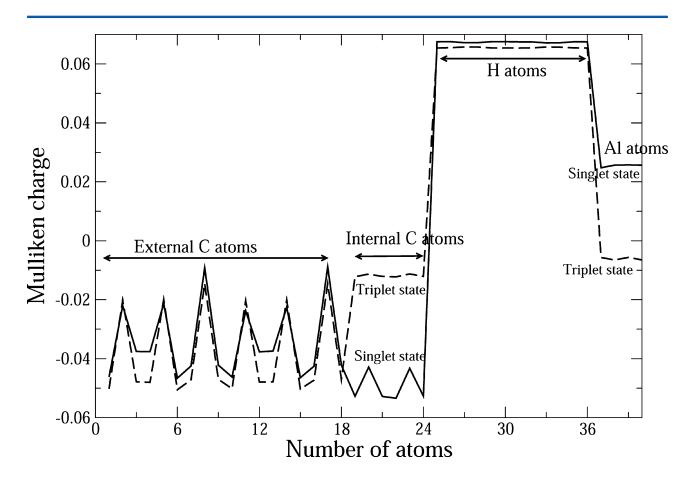


Figure 3. Mulliken charges on the Al_4 cluster interacting with coronene as shown in Figure 2. The x axis shows the number of atoms. Atoms 0–18, 19–24, 25–36, and 37–40 correspond to the external C atoms, the internal C atoms, the external hydrogen atoms, and the four aluminum atoms of the Al_4 –C in Figure 2b, respectively.

Mulliken charges of the Al₄–C system for the singlet and the triplet state. The C atoms placed in the middle of the coronene surface (atom numbers 19–23) and interacting directly with the aluminum cluster (atom numbers 37–40) have in the singlet state an absolute Mulliken charge larger than the charge of the external C atoms and the aluminum atoms. This phenomenon is absent in the triplet state, where the Mulliken charge is similar for the aluminum atoms and the internal C atoms. As discussed further below, this, together with the short Al–C distance, is the reason for the extra stability of the Al₄–C system in the singlet state.

A calculation of the electrostatic part of the interaction energy between the cluster and the molecule shows how part of the stabilization of the singlet state is through charge transfer. We calculated the electrostatic energy for the Al_4 –C complex in the singlet and the triplet state using:

$$E_{\text{elec}} = \sum_{i=1}^{n_{\text{C}}} \sum_{j=1}^{n_{\text{Al}}} q_i q_j / R_{ij}$$
(4)

where the q_i 's are the Mulliken charges, and the values obtained for the $^1\text{Al}_4$ –C and $^3\text{Al}_4$ –C systems are -0.094 and -0.017 eV, respectively, in agreement with the idea that a small charge transfer exists between the Al atoms and the C molecule.

The highest occupied molecular orbital (HOMO, data not shown) for the 1 Al₄–C, shows that its electron density is mostly localized in the space between C and the aluminum cluster: this suggests the presence of a weak bond of covalent character in addition to the already noted charge transfer. From the population analysis, the coefficients of molecular orbitals show that the main atomic orbitals forming the HOMO are the s, p_x , and p_y orbitals of the four aluminum atoms. It is also interesting to note the distribution of the spin population in the triplet state of the Al₄–C system. Although the triplet Al₄–C state presents the same charge distribution on the internal carbons and on the aluminum atoms of the coronene, the spin population is mainly localized on the aluminum atoms.

We now proceed to the analysis of the Al_n –G interaction. The interaction of the Al_n cluster with G may occur through physisorption or chemisorption, where the physisorption interaction involves a possible charge transfer⁶³ and does not involve a chemical bond, thereby preserving graphene's intrinsic π bond structure. The analysis of the binding energies, the distances, and the molecular orbitals involved, is consistent with an interaction intermediate between chemisorption and physisorption.

Figure 4 shows the minimum energy structures of Al_2 –G, Al_4 –G, and Al_6 –G. Relative to the Al_2 cluster on C, the Al–Al distance increases from 2.81 to 2.92 Å and the graphene C–C bonds underneath the Al_2 are the same at 1.44 Å, with Al–C distances of 2.38 Å, indicating an interaction stronger than a usual physisorption interaction. Since G is an infinite surface, the edge/field gradient effect observed for Al_2 –C is no longer present. Al_2 on G prefers to sit more or less parallel to a C–C bond.

The Al_4 –G and Al_6 –G cases present different scenarios. The Al–Al distances are longer than in the bare Al_n cluster (2.60 and 2.70 Å for Al_4 –G and Al_6 –G, respectively), but still shorter than in the Al_n on C, though only by a small amount for Al_6 . The distance between the Al_n cluster and the C atoms of G is around 4.0 Å. The interaction of Al_n with G does not affect the conformations of the Al_4 and Al_6 clusters, although the Al_6 cluster rotates to match to at least two C atoms of the surface. The similar Al–Al and Al–C distances for the Al_4 –C and Al_6 –C correlate with similar binding energies (–0.66 and –0.55 eV compared to –0.75 and –0.47 eV for Al_n –C, respectively).

The interaction of the Al_2 and Al_4 in the singlet state is stronger with the C molecule than with the G surface, and this result is supported by CT, electrostatic energy, and molecular orbital analysis. Moreover, the CT in the $Al_{2,4}$ –C systems from the Al atoms toward the C molecule is enhanced by the curvature of the C molecule itself, and by the short Al–C distances of 2.09 and 2.82 Å in the Al_2 –C and Al_4 –C systems, respectively. This result affects the dissociation energy of the H_2 molecule, as we will discuss in the next section and it is in agreement with previous work.²³ Moreover, the inclusion of dispersion interactions is important to describe our model, as has been found also by Lazar et al.⁶⁴ for small organic molecules on coronene and graphene. They also found that

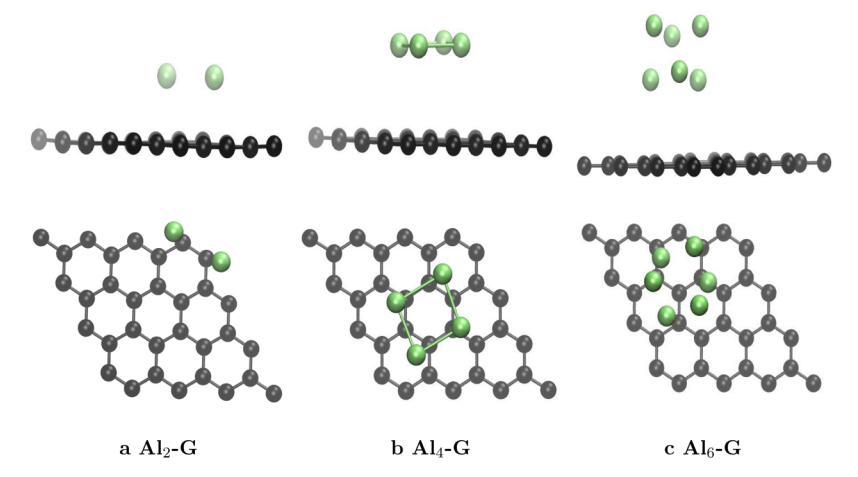


Figure 4. Al_n with n = 2, 4, and 6 atoms interacting with graphene (G). Side and top views are shown in the first and second row, respectively. Black and dark gray (green) balls correspond to the C and Al atoms, respectively.

dispersive and electrostatic interactions play the main role for these kinds of systems using symmetry-adapted perturbation theory, which includes dispersion, induction and electrostatic interactions.

C. Chemisorbed States of H_2 on Al_n Supported by Carbon Materials (C and G). Before exploring the minimum energy paths describing the dissociation of an H_2 molecule on the system Al_n -S, we studied the chemisorbed configurations of H_2 on the Al_n -S system, where S can be either C or G.

Since H atoms can chemisorb on the Al_n cluster in different positions, we tried a range of configurations of the H_2 molecule dissociated on Al_n surfaces supported by carbon materials. As mentioned before, we have observed that the coronene molecule stabilizes the singlet state of the Al_n cluster with respect to the triplet state, so we performed the calculations only on the singlet states of the hydrogenated systems.

Figures 5 and 6 show the optimized structures of H_2 dissociated on Al_n clusters on C and G, respectively. Among all of the configurations studied, the most stable ones are the ones where the two H atoms are positioned along a line perpendicular to an Al–Al bond, forming a four-center motif with these two Al atoms (see for instance Figure 5a).

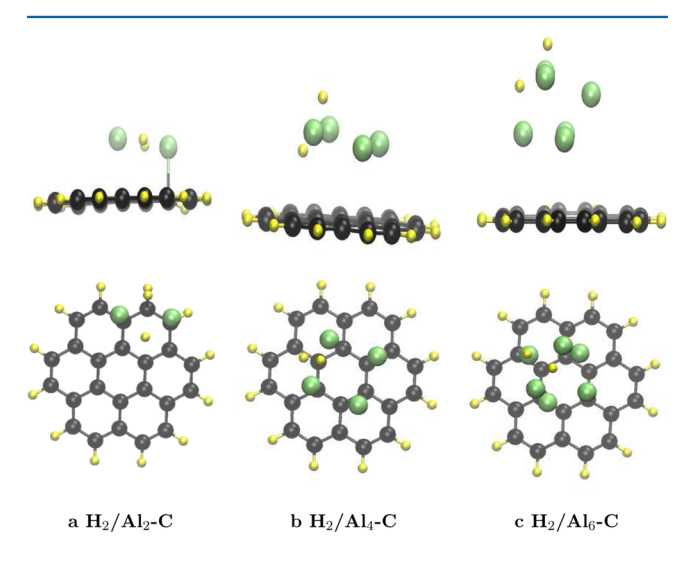


Figure 5. Dissociated H_2 molecule on Al_n with n = 2, 4, and 6 atoms interacting with coronene (C). Black, light gray (yellow), and dark gray (green) balls correspond to the C, H, and Al atoms, respectively.

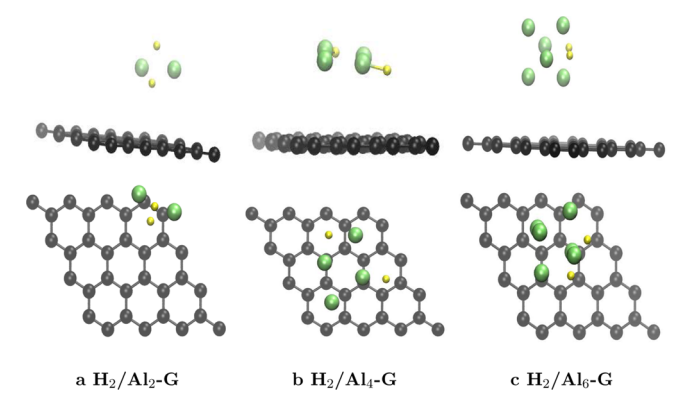


Figure 6. Dissociated H_2 molecule on aluminum clusters with 2, 4, and 6 atoms interacting with graphene (G). Black, light gray (yellow), and dark gray (green) balls correspond to the C, H, and Al atoms, respectively.

In Table 2, we can observe how the Al–Al distance changes going from the bare Al_n cluster, via Al_n –C and Al_n –G, to the hydrogenated systems (H_2 – Al_n –C and H_2 – Al_n –G).

We start by analyzing the H_2 – Al_2 –C system. The Al–Al distance decreases from 3.10 to 2.81 and further to 2.80 Å for the bare Al_2 cluster, Al_2 –C, and H_2 – Al_2 –C, respectively. Note that the C molecule is no longer deformed after the H_2 dissociation on Al_2 (Figure 5a) in contrast to the case where H atoms are not present (Figure 2a).

For the $\rm H_2$ – $\rm Al_4$ – $\rm C$ system, the Al–Al distance varies from 2.48 to 2.66 to 2.54 Å for the Al₄ cluster, Al₄– $\rm C$, and $\rm H_2$ –Al₄– $\rm C$, respectively. In this case, the deformation of the Al₄ cluster upon binding with the $\rm H_2$ is smaller than in Al₄– $\rm C$ (compare Figures 5b and 2b).

Finally for the $\rm H_2$ – $\rm Al_6$ – $\rm C$ system, the Al–Al distance increases from 2.57 to 2.71 and then decreases to 2.57 Å going from Al₆ to Al₆– $\rm C$ and to $\rm H_2$ – $\rm Al_6$ – $\rm C$, respectively.

The distance between the Al_n cluster and C atoms follows the same trend for all the systems studied. The Al-C distance decreases from 3.68 to 3.25 Å going from Al_6-C to H_2-Al_6-C , respectively, as a result of the formation of a strong covalent bond between the two H atoms and two Al atoms of the cluster (see Figure 5c). The H-Al distances range from 1.7 to 1.9 Å.

Table 4 reports the binding energies of the most stable structures found for the H_2 – Al_n –C and H_2 – Al_n –G complexes, calculated with respect to the H_2 molecule:

Table 4. Binding Energies (eV) Calculated by eq 5 for H_2 Chemisorbed on Al_n Clusters Interacting with C and G^a

	functional		
system	PBE	vdW-DF	B3LYP
H_2 - Al_2 - C	-1.01	-0.98	-1.21
H_2-Al_4-C	-1.55	-1.21	-1.26
H_2 - Al_6 - C	-1.14	-0.71	-0.98
H_2-Al_2-G	-1.32	-1.10	
H_2 - Al_4 - G	-0.95	-0.88	
H_2-Al_6-G	-0.99	-0.72	

"See Figures 5 and 6. DFT calculations with pure PBE, vdW-DF, and B3LYP functionals are reported.

$$E_{\rm b} = E_{\rm (H2-Aln-S)} - E_{\rm (Aln-S)} - E_{\rm (H2)}$$
 (5)

As already noticed from our calculations on the bare Al_n clusters, pure PBE calculations yield larger E_b than the vdW-DF and B3LYP calculations, while good agreement has been found between vdW-DF and B3LYP calculations. This is in line with previous results, ⁶⁴ and highlights the crucial importance of using nonlocal electron correlation at the DFT level.

Now we discuss the hydrogenated Al_n cluster on the G surface. Analyzing the various chemisorbed configurations, some similaries can be found between H_2 on Al_n on C and on G. In fact, the Al–Al distance changes from 3.10 to 2.92 to 2.54 Å for Al_2 , Al_2 on G, and H_2 – Al_2 –G, respectively. Similarly for the Al_4 cluster, the Al–Al distance changes from 2.48 to 2.60 to 2.50 Å for Al_4 , Al_4 on G, and H_2 – Al_4 –G, respectively.

Finally, for the Al₆ cluster, the Al-Al distance changes from 2.57 Å in the bare cluster to 2.70 Å in Al₆ on G to 2.62 Å in H₂-Al₆-G. The Al-C atom distance is around 4.0 Å for the latter two systems indicating a weaker interaction of Al₆ with G than with the C molecule. Moreover, in all the hydrogenated systems interacting with the G surface, a strong covalent bond is formed between the two H atoms and the Al atoms. The corresponding distances range from 1.6 to 1.9 Å, very similar to the C case. Comparing Figures 5 and 6, the similarity is evident between the hydrogenated configurations with the two different carbon materials. An exception is observed for Figures 5b and 6b, where the two H atoms on the graphene surface do not form the usual four-center motif, but a bridge is formed by two Al atoms and one H atom, and a covalent bond is formed between H-Al on the opposite side. In Figures 5c and 6c, the two H atoms still form the four-center motif but the Al6 cluster rearranges on graphene in a more symmetric way than on the coronene molecule.

D. Hydrogen Dissociation on Al_n Supported by Carbon Materials (C and G). Finally, we have calculated the activation barriers for dissociation of H_2 on Al_n —C and Al_n —G. Our goal is to see the effect of the carbon materials on the dissociation of H_2 on Al_n clusters.

In order to evaluate the activation barriers we performed NEB calculations. As we have mentioned before, the Al_n clusters, when interacting with C_n are stabilized in the singlet state. This is the reason why we studied all the reaction paths for singlet dissociation of H_2 on a C or G support. All the initial and final configurations, needed by NEB to find the minimum energy reaction paths, were optimized with PW basis set and vdW-DF functional. Table 5 and Figures 7 and 8 show the activation energy barriers and the corresponding minimum energy paths for H_2 on bare Al_n-C_n , and on Al_n-G_n , respectively. In all of the minimum energy reaction paths studied, the

Table 5. Activation Energy Barrier Heights (eV) Calculated by NEB for the Dissociation of H_2 on the C Molecule and on the G Surface^a

	H_2 on Al_n	H ₂ on Al _n -C	H ₂ on Al _n -G
Al_2	0.69^{a}	0.41	0.45
Al_4	0.50^{a}	0.0	0.17
Al_6	0.07^{a}	0.0	0.15

^aThe reaction paths on C and on G are shown in Figures 7 and 8, respectively. Values^a of activation energy barriers (eV) on the bare Al_n clusters are taken from ref 30.

starting point is a physisorbed state, obtained by geometry optimization at a local (metastable) minimum, in which the H_2 molecule is placed ~3.0 Å from the Al_n cluster, and the final state is represented by the dissociated chemisorbed state of the H_2 molecule as discussed in the previous section. Figure 7 shows the dissociation of H_2 on the Al_n –C surface with n=2, 4, and 6.

In our analysis we can distinguish two effects: the effect of the cluster size (2, 4, or 6 Al atoms) and of the carbon material (C or G). Increasing the Al cluster size on the C molecule from two to four makes the dissociation of H_2 barrierless. This is a very interesting result that demonstrates the catalytic effect due to the carbon material as suggested from experiments. The dissociation of H_2 on Al_2 –C shows an activation barrier of 0.41 eV. This value is already lower than for H_2 dissociation on the bare Al_2 cluster (0.69 eV). The transition state is characterized by the lenghtening of the H–H distance from 0.75 to 1.06 Å with the Al–Al distance still at the initial value (2.80 Å).

Already for the Al_4 cluster on C, the dissociation of H_2 molecule is barrierless, i.e., the H_2 molecule is already dissociated in the second image of the reaction path, reaching the position above and under the Al–Al side of the Al_4 cluster, and reproducing once again the four center motif. It is interesting to note that Al_4 was perfectly square before interacting with the H_2 molecule and the Al–Al bond, involved in the four center motif, decreases from 2.64 to 2.54 Å when the 2 H atoms lie in this motif.

The coronene molecule adopts a bell-shaped geometry in the first image with a dihedral angle of 20° but becomes completely planar by the last image. To verify the lack of activation energy of this pathway, we computed a reaction path starting from the H_2 molecule placed at 7 Å from the surface and ending in the final physisorbed configuration at 3 Å. The results show a barrierless process. Calculations with the B3LYP functional using the previously described configurations confirm this result. As noticed by Berseth et al. ²³ the curvature of the carbon material is directly connected with its electronic affinity (EA) and with the release of the H in the NaAlH₄. By analogy, we observe that the curvature of the coronene molecule in the Al_4 –C system, together with a CT from the Al atoms toward the surface, promotes the dissociation of H_2 for the Al_4 –C system, making it barrierless.

The dissociation of $\rm H_2$ on $\rm Al_6-C$ also shows a barrierless reaction path. The starting point is characterized by $\rm Al_6$ with the gas phase equilibrium structure above the C molecule and an Al-C distance of 4.0 Å. The second image of this reaction path already shows the dissociation of $\rm H_2$ on the $\rm Al_6$, and only at the last step the two H atoms reform part of the typical four center motif, with an H–Al distance of 1.90 Å and Al–C distance of ~4.5 Å.

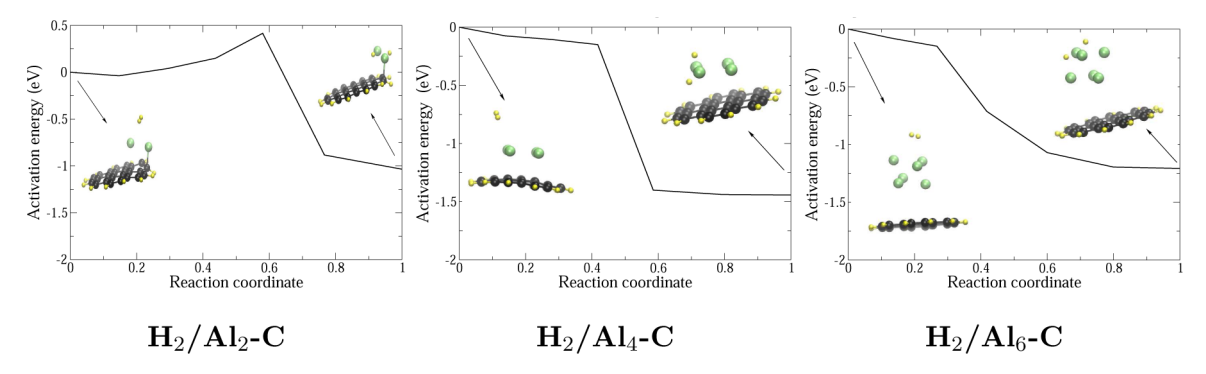


Figure 7. Minimum energy dissociation pathway of H_2 molecule on Al_n clusters with n = 2, 4, and 6 atoms interacting with coronene (C). All of the calculations were performed by NEB. The initial and final state, shown in the figures (see also Figure 5), correspond to the physisorbed and chemisorbed state of H_2 on $Al_n - C$, respectively.

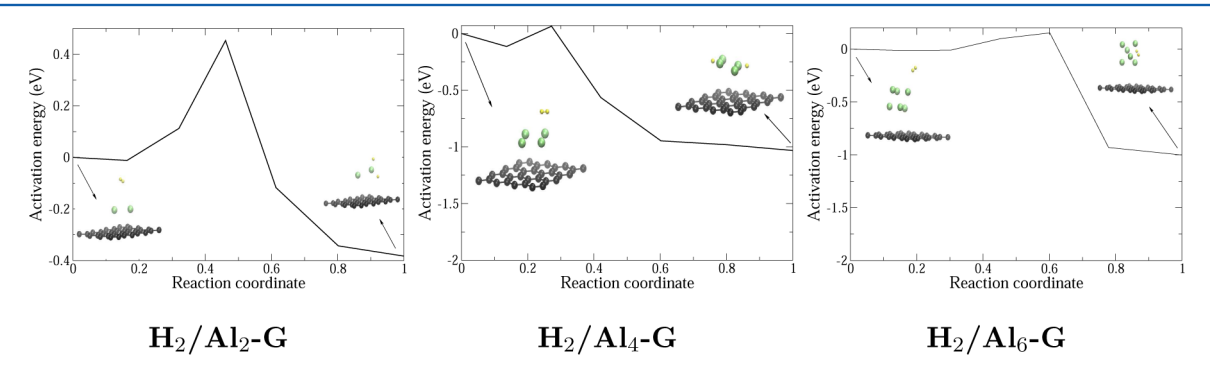


Figure 8. Minimum energy dissociation pathway of H_2 molecule on Al_n clusters with n = 2, 4, and 6 atoms interacting with graphene (G). All of the calculations were performed by NEB. The initial and final state, shown in the figures (see also Figure 6), correspond to the physisorbed and chemisorbed state of H_2 on $Al_n - G$, respectively.

Considering the infinite surface of graphene, some differences between this surface and the coronene molecule become apparent. Figure 8 shows the dissociation of H_2 on Al_n —G with n=2, 4, and 6. The Al_2 on G shows the promoting effect of the G surface with respect to the bare Al_2 cluster. The reaction path is similar to the path observed for H_2 on Al_2 —C, with a similar barrier (0.45 eV). The interesting difference is that on the G surface the H_2 molecule prefers to dissociate on one Al atom, forming a three center motif instead of a four center motif. The H atoms are equidistant at 1.61 Å from the same Al atom. The Al—Al distance decreases from 2.85 to 2.80 Å while the interaction between the Al and C atoms becomes weaker, and the distance increases to 4.0 Å. The transition state of this reaction path is characterized by an H—H distance of 0.77 Å.

For Al_4 , the H_2 molecule dissociates with a very low barrier (0.17 eV) and reaches a final configuration with the two H atoms much further apart than for the bare Al_4 cluster, with one H bridging two Al atoms and another H atom covalently linked to the other Al atom at a distance of 1.59 Å. The final structure maintains the same distance of the Al cluster from the G, although the Al_4 rearranges completely, with the internal angles changing from 106° to 116° and from 72° to 61° with respect to the initial state, so that they match up with two C atoms of the surface.

The dissociation of $\rm H_2$ on $\rm Al_6-G$ is characterized by a very low barrier (0.15 eV), and a final distance $\rm Al-G$ of 3.9 Å. Following the reaction path, while the H–H distance increases, the $\rm Al_6$ cluster rotates on the G surface of ~20° clockwise, keeping its cyclohexane structure and increasing the distance with the surface in the final structure. The two H atoms become part of the four center motif. The two H atoms form a

covalent bond with two Al atoms, increasing the Al–G distance from 3.60 to 3.90 Å.

The effect of the infinite G surface interacting with Al_4 cluster is to lower the barrier from 0.50 eV up to 0.17 eV for dissociation of H_2 , whereas the H_2 dissociation over Al_4 on C is barrierless. This result is in line with previous work²³ and can be explained by the lack or minimal distortion of the graphene surface. We see that in all cases except Al_6 —G the presence of the carbon surface lowers the barrier to dissociation of H_2 over Al_n . Also, for Al_6 the barrier is already quite low for the bare cluster. The results show that the presence of C promotes the dissociation of H_2 over small Al_n clusters with n even. The finding that the coronene molecule, which also exhibits edges, promotes the dissociation more than graphene is consistent with the experimental observation that carbon nanofibers exhibit an expecially large catalystic effect on hydrogen release from NaAlH4.

IV. CONCLUSIONS

In this paper we demonstrate, using DFT and by NEB calculations, the promoting effect that carbon materials, i.e., coronene and graphene, have on the dissociation of H_2 over Al_n clusters. The PBE GGA was used together with vdW interactions in both spin unpolarized and polarized calculations. We attempt to explain a key experimental finding that hydrogen adsorption properties of sodium alanate (NaAlH₄) are markedly improved by the presence of nanoporous carbon. We used coronene and graphene as models for nanosized carbon materials. As described in the Introduction, coronene is a suitable molecule to mimic the effect of the edge (defect) of nanocarbon surfaces such as carbon nanofibers on H_2

dissociation. We show that the finite extent of the C molecule facilitates, the deformation of the molecule bound to the Al atoms of the cluster. This interaction of the C molecule with Al, clusters stabilizes the Al clusters in the singlet state for any cluster size, which is the most favorable one for H₂ dissociation. The overstabilization of ¹Al_n-C relative to ³Al_n-C is due to both physisorption and chemisorption interactions, and for ≈20% to a CT between the Al atoms and the C molecule. For the Al₄-C systems the effect of the curvature of the coronene molecule, together with a CT from Al toward the C atoms, promotes the dissociation of the H2 molecule so that it becomes barrierless over the supported Al₄ cluster. For the graphene surface, the effect of the infinite surface is to lower the barrier from 0.50 to 0.17 eV for the dissociation of H₂ on Al₄-G. The difference between this and coronene as a substrate can be explained by the lack or minimal distortion of the graphene surface. Similar results were found for C₆₀, carbon nanotubes, and graphene interacting with a NaAlH₄ cluster. ²³ In the former case the curvature of the C₆₀ is strongly related to the electronic affinity of the surface itself, demonstrating that in this case the curvature of the surface promotes the release of the H atom with respect to other carbon materials.

AUTHOR INFORMATION

Corresponding Author

*E-mail: costanzof@chem.leidenuniv.nl.

Notes

The authors declare no competing financial interest.

ACKNOWLEDGMENTS

We thank Dr. Ilaria Pino for performing the groundwork for this project and ACTS-CW for funding this research as part of the "Sustainable Hydrogen program".

REFERENCES

- (1) Paster, M. D.; Ahluwalia, R. K.; Berry, G.; Elgowainy, A.; Lasher, S.; McKenney, K.; Gardiner, M. Hydrogen Storage Technology Options for Fuel Cell Vehicles: Well-to-Wheel Costs, Energy Efficiencies, and Greenhouse Gas Emissions. *Int. J. Hydrogen Energy* **2011**, *36*, 14534–14551.
- (2) Felderhoff, M.; Weidenthaler, C.; von Helmolt, R.; Eberle, U. Hydrogen Storage: the Remaining Scientific and Technological Challenges. *Phys. Chem. Chem. Phys.* **2007**, *9*, 2643–2653.
- (3) McWhorther, S.; Read, C.; Ordaz, G.; Stetson, N. Materials-Based Hydrogen Storage: Attributes for Near-Term, Early Market PEM Fuel Cells. *Curr. Opin. Solid State Mater. Sci.* **2011**, *15*, 29–38.
- (4) Yadav, M.; Xu, Q. Liquid-Phase Chemical Hydrogen Storage Materials. *Energy Environ. Sci.* **2012**, *5*, 9698–9725.
- (5) Struzhkin, V. V.; Militzer, B.; Mao, W. L.; Mao, H.-K.; Hemley, R. J. Hydrogen Storage in Molecular Clathrates. *Chem. Rev.* **2007**, *107*, 4133–4151.
- (6) Rowsell, J. L. C.; Yaghi, O. M. Strategies for Hydrogen Storage in Metal-Organic Frameworks. *Angew. Chem., Int. Ed.* **2005**, 44, 4670–4679
- (7) Liu, C.; Fan, Y. Y.; Liu, M.; Cong, H. T.; Cheng, H. M.; Dresselhaus, M. S. Hydrogen Storage in Single-Walled Carbon Nanotubes at Room Temperature. *Science* **1999**, 286, 1127–1129.
- (8) Dehouche, Z.; Lafi, L.; Grimard, N.; Goyette, J.; Chahine, R. The Catalytic Effect of Wingle-Wall Carbon Nanotubes on the Hydrogen Sorption Properties of Sodium Alanates. *Nanotechnology* **2005**, *16*, 402–409.
- (9) Orimo, S.-I.; Nakamori, Y.; Eliseo, J. R.; Zuttel, A.; Jensen, C. M. Complex Hydrides for Hydrogen Storage. *Chem. Rev.* **2007**, *107*, 4111–4132.

- (10) Jena, P. Materials for Hydrogen Storage: Past, Present, and Future. J. Phys. Chem. Lett. 2011, 2, 206–211.
- (11) von Helmolt, R.; Eberle, U. Fuel Cell Vehicles: Status 2007. J. Power Sources 2007, 165, 833–843.
- (12) Jorgensen, S. W. Hydrogen Storage Tanks for Vehicles: Recent Progress and Current Status. *Curr. Opin. Solid State Mater. Sci.* **2011**, 15, 39–43.
- (13) Weidenthaler, C.; Felderhoff, M. Solid-State Hydrogen Storage for Mobile Applications: Quo Vadis? *Energy Environ. Sci.* **2011**, *4*, 2495–2502.
- (14) Bogdanović, B.; Schwickardi, M. Ti-Doped Alkali Metal Aluminium Hydrides as Potential Novel Reversible Hydrogen Storage Materials. *J. Alloys Compd.* **1997**, 253, 1–9.
- (15) Bogdanović, B.; Brand, R. A.; Marjanovic, A.; Schwickardi, M.; Tolle, J. Metal-Doped Sodium Aluminium Hydrides as Potential New Hydrogen Storage Materials. *J. Alloys Compd.* **2000**, *302*, *36*–58.
- (16) Frankcombe, T. J. Proposed Mechanisms for the Catalytic Activity of Ti in NaAlH₄. Chem. Rev. 2012, 112, 2164–2178.
- (17) Marashdeh, A.; Olsen, R. A.; Løvvik, O. M.; Kroes, G.-J. A Density Function Theory Study of Ti-Doped NaAlH₄ Clusters. *Chem. Phys. Lett.* **2006**, 426, 180–186.
- (18) Marashdeh, A.; Versluis, J.-W. I.; Valdés, A.; Olsen, R. A.; Løvvik, O. M.; Kroes, G.-J. Effect of Transition Metal Dopants on Initial Mass Transport in the Dehydrogenation of NaAlH4: Density Functional Theory Study. *J. Phys. Chem. C* **2013**, *117*, 3–14.
- (19) Balde, C. P.; Stil, H. A.; van der Eerden, A. M. J.; de Jong, K. P. Bitter, J. H. Active Ti Species in TiCl₃-Doped NaAlH₄. Mechanism for Catalyst Deactivation. *J. Phys. Chem. C* **2007**, *111*, 2797–2802.
- (20) Haiduc, A. G.; Stil, H. A.; Schwarz, M. A.; Paulus, P.; Geerlings, J. J. C. On the Fate of the Ti Catalyst During Hydrogen Cycling of Sodium Alanate. *J. Alloys Compd.* **2005**, 393, 252–263.
- (21) Majzoub, E. H.; Gross, K. J. Titanium-Halide Catalyst-Precursors in Sodium Aluminum Hydrides. *J. Alloys Compd.* **2003**, 356, 363–367.
- (22) Leon, A.; Kircher, O.; Rösner, H.; Décamps, B.; Leroy, E.; Fichtner, M.; Percheron-Guégan, A.; SEM, T. E. M. Characterization of Sodium Alanate Doped with TiCl₃ or Small Ti Clusters (Ti₁3*6THF). *J. Alloys Compd.* **2006**, 414, 190–203.
- (23) Berseth, P. A.; Harter, A. G.; Zidan, R.; Blomqvist, A.; Araújo, C. M.; Scheicher, R. H.; Ahuja, R.; Jena, P. Carbon Nanomaterials as Catalysts for Hydrogen Uptake and Release in NaAlH₄. *Nano Lett.* **2009**, *9*, 1501–1505.
- (24) Adelhelm, P.; de Jongh, P. E. The Impact of Carbon Materials on the Hydrogen Storage Properties of Light Metal Hydrides. *J. Mater. Chem.* **2011**, *21*, 2417–2427.
- (25) Balde, C. P.; Hereijgers, B. P. C. Bitter, J. H.; de Jong, K. P. Facilitated Hydrogen Storage in NaAlH₄ Supported on Carbon Nanofibers. *Angew. Chem., Int. Ed.* **2006**, *45*, 3501–3503.
- (26) Adelhelm, P.; de Jong, K. P.; de Jongh, P. E. How Intimate Contact with Nanoporus Carbon Benefits the Reversible Hydrogen Desorption from NaH and NaAlH₄. *Chem. Commun.* **2009**, *41*, 6261–6263.
- (27) Gao, J.; Ngene, P.; Lindemann, I.; Gutfleisch, O.; de Jong, K. P.; de Jongh, P. E. Enhanced Reversibility of H₂ Sorption in Nanoconfined Complex Metal Hydrides by Alkali Metal Addition. *J. Mater. Chem.* **2012**, 22, 13209–13215.
- (28) Moc, J. Hydrogenation of Aluminium Hexamer: Ab Initio Molecular Orbital Theory and Density Functional Theory Study. *Chem. Phys. Lett.* **2008**, *466*, 116–121.
- (29) Moc, J. Reactivity of Aluminium Dimer with H_2 : the Performance of High Level ab initio and Density Functional Methods for Prediction of Reaction Paths. *Chem. Phys. Lett.* **2005**, 401, 497–502.
- (30) Pino, I.; Kroes, G.-J.; van Hemert, M. C. Hydrogen Dissociation on Small Aluminum Clusters. J. Chem. Phys. 2010, 133, 184304.
- (31) Kawamura, H.; Kumar, V.; Sun, Q.; Kawazoe, Y. Magic Behavior and Bonding Nature in Hydrogenated Aluminum Clusters. *Phys. Rev. B* **2001**, *65*, 045406–11.

- (32) Giannozzi, P.; et al. Quantum ESPRESSO: a Modular and Open-Source Software Project for Quantum Simulations of Materials. *J. Phys.: Condens. Matter* **2009**, *21*, 395502.
- (33) Perdew, J. P.; Burke, K.; Ernzerhof, M. Generalized Gradient Approximation Made Simple. *Phys. Rev. Lett.* **1996**, *77*, 3865–3868.
- (34) Mermin, N. D. The Catalytic Effect of Single-Wall Carbon Nanotubes on the Hydrogen Sorption Properties of Sodium Alanates. *Phys. Rev.* **1965**, *137*, A1441.
- (35) Version 2.2. CP2K is freely available from www.cp2k.org
- (36) Goedecker, S.; Teter, M.; Hutter, J. Separable Dual Space Gaussian Pseudo-Potentials. *Phys. Rev. B* **1996**, *54*, 1703–1710.
- (37) Frisch, M. J.; et al. *Gaussian 03*, revision C.02; Gaussian Inc.: Wallingford CT, 2004.
- (38) Becke, A. D. Density-Functional Exchange-Energy Approximation with Correct Asymptotic-Behavior. *Phys. Rev. A* **1988**, 38, 3098–3100.
- (39) Lee, C.; Yang, W.; Parr, R. Development of the Colle-Salvetti Correlation-Energy Formula into a Functional of the Electron Density. *Phys. Rev. B* **1988**, *37*, 785–789.
- (40) Henkelman, G.; Jónsson, H. Improved Tangent Estimate in the Nudged Elastic Band Method for Finding Minimum Energy Paths and Saddle Points. *J. Chem. Phys.* **2000**, *113*, 9978–9985.
- (41) Broyden, C. G. Quasi-Newton Methods and their Application to Function Minimisation. *Math. Comput.* **1967**, *21*, 368–381.
- (42) Dion, M.; Rydberg, H.; Schröder, E.; Langreth, D.; Lundqvist, B. Van der Waals Density Functional for General Geometries. *Phys. Rev. Lett.* **2004**, *92*, 246401–246404.
- (43) Grimme, S. Accurate Description of Van der Waals Complexes by Density Functional Theory Including Empirical Corrections. *J. Comput. Chem.* **2004**, *25*, 1463–1473.
- (44) Ma, J.; Michaelides, A.; Alfé, D. Binding of Hydrogen on Benzene, Coronene, and Graphene from Quantum Monte Carlo Calculations. *J. Chem. Phys.* **2011**, *134*, 134701–134706.
- (45) Ma, J.; Michaelides, A.; Alfé, D.; Schimka, L.; Kresse, G.; Wang, E. Adsorption and Diffusion of Water on Graphene from First Principles. *Phys. Rev. B* **2011**, *84*, 033402–4.
- (46) Klimeš, J.; Bowler, D. R.; Michaelides, A. Chemical Accuracy for the van der Waals Density Functional. *J. Phys.: Condens. Matter* **2010**, 22, 022201–5.
- (47) Mura, M.; Gulans, A.; Thonhauser, T.; Kantorovich, L. Role of van der Waals Interaction in Forming Molecule-Metal Junctions: Flat Organic Molecules on the Au(111) Surface. *Phys. Chem. Chem. Phys.* **2010**, *12*, 4759–4767.
- (48) Li, G.; Tamblyn, I.; Cooper, V. R.; Gao, H.-J.; Neaton, J. B. Molecular Adsorption on Metal Surfaces with van der Waals Density Functionals. *Phys. Rev. B* **2012**, *85*,121409-4(R).
- (49) Carrasco, J.; Klimeš, J.; Michaelides, A. The Role of van der Waals Forces in Water Adsorption on Metals. *J. Chem. Phys.* **2013**, 138, 024708–9.
- (50) Carrasco, J.; Santra, B.; Klimeš, J.; Michaelides, A. To Wet or Not to Wet? Dispersion Forces Tip the Balance for Water Ice on Metals. *Phys. Rev. Lett.* **2011**, *106*, 026101–4.
- (51) Medeiros, P. V. C.; Gueorguiev, G. K.; Stafström, S. Benzene, Coronene, and Circumcoronene Adsorbed on Gold, and Gold Cluster Adsorbed on Graphene: Structural and Electronic Properties. *Phys. Rev. B* **2012**, *85*, 205423–7.
- (52) Gobre, V. V.; Tkatchenko, A. Scaling Laws for Van der Waals Interactions in Nanostructured Materials. *Nat. Commun.* **2013**, *4*, 2341.
- (53) Ruiz, V. G.; Liu, W.; Zojer, E.; Scheffler, M.; Tkatchenko, A. Density-Functional Theory with Screened Van der Waals Interactions for the Modeling of Hybrid Inorganic-Organic Systems. *Phys. Rev. Lett.* **2012**, *108*, 146103–5.
- (54) Tkatchenko, A.; Romaner, L.; Hofmann, O. T.; Zojer, E.; Ambrosch-Draxl, C.; Scheffler, M. Van der Waals Interactions Between Organic Adsorbates and at Organic/Inorganic Interfaces. *MRS Bull.* **2010**, *35*, 435–442.

- (55) Schultz, N. E.; Staszewska, G.; Staszewski, P.; Truhlar, D. G. Validation of Theoretical Methods for the Structure and Energy of Aluminum Clusters. *J. Phys. Chem. B* **2004**, *108*, 4850–4861.
- (56) Fu, Z. W.; Lemire, G. W.; Hamrick, Y. M.; Taylor, S.; Shui, J. C.; Morse, M. Spectroscopic Studies of the Jet-Cooled Aluminum Trimer. *J. Chem. Phys.* **1988**, *88*, 3524–3531.
- (57) Fu, Z. W.; Lemire, G. W.; Bishea, G. A.; Morse, M. D. Spectroscopy and Electronic-Structure of Jet-Cooled Al₂. *J. Chem. Phys.* **1990**, 93, 8420–8441.
- (58) Fu, Z. W.; Russon, L. M.; Morse, M. D.; Armentrout, P. B. Photodissociation Measurements of Bond Dissociation Energies: $D0(Al_2-Al)$, $D0(TiO^+-Mn)$, and $D0(V_2^+-V)$. Int. J. Mass. Spectrom. **2001**, 204, 143–157.
- (59) Costanzo, F.; Silvestrelli, P. L.; Ancilotto, F. Physisorption, Diffusion, and Chemisorption Pathways of H₂ Molecule on Graphene and on (2,2) Carbon Nanotube by First Principles Calculations. *J. Chem. Theory Comput.* **2012**, *8*, 1288–1294.
- (60) Costanzo, F.; Silvestrelli, P. L.; Scipioni, R.; Ancilotto, F. Interaction of H₂ with a Double Walled Armchair Nanotube by First Principles Calculations. 2013, submitted.
- (61) Li, X.; Eustis, S.; Bowen, K. H.; Kandalam, A. K.; Jena, P. Photoelectron Spectroscopic and Theoretical Studies of Fe(m) (Coronene)n (m=1,2, n=1,2) Complexes. *J. Chem. Phys.* **2008**, *129*, 074313.
- (62) Khanna, S. N.; Jena, P. Assembling Crystals from Clusters. *Phys. Rev. Lett.* **1992**, *69*, 1664–1667.
- (63) Gong, C.; Lee, G.; Shan, B.; Vogel, E. M.; Wallace, R. M.; Cho, K. First Principles Study of Metal-Graphene Interfaces. *J. Appl. Phys.* **2010**, *108*, 123711–123718.
- (64) Lazar, P.; Karlický, F.; Jurečka, P.; Kocman, M.; Otyepková, E.; Šafářová, K.; Otyepka, M. Adsorption of Small Organic Molecules on Graphene. *J. Am. Chem. Soc.* **2013**, *135*, 6372–6377.